JGR Atmospheres

RESEARCH ARTICLE
10.1029/2022JD036935

A Multi-Algorithm Analysis of Projected Changes to Freezing Rain Over North America in an Ensemble of Regional Climate Model Simulations

Christopher D. McCray[1,2], Dominique Paquin[1], Julie M. Thériault[2], and Émilie Bresson[1,2]

[1]Ouranos, Montréal, QC, Canada, [2]Centre pour l'Étude et la Simulation à l'Échelle Régionale (ESCER), Department of Earth and Atmospheric Sciences, Université du Québec à Montréal, Montréal, QC, Canada

Key Points:

- Freezing rain is projected to increase in frequency over portions of western and central Canada and decrease over most of the United States
- The sign of projected changes is not highly sensitive to the precipitation-type algorithm used to diagnose freezing rain
- The choice of driving global climate model is a key source of uncertainty in both the sign and magnitude of projected changes

Correspondence to:
C. D. McCray,
mccray.christopher@ouranos.ca

Citation:
McCray, C. D., Paquin, D., Thériault, J. M., & Bresson, É. (2022). A multi-algorithm analysis of projected changes to freezing rain over North America in an ensemble of regional climate model simulations. *Journal of Geophysical Research: Atmospheres*, *127*, e2022JD036935. https://doi.org/10.1029/2022JD036935

Received 13 APR 2022
Accepted 30 JUN 2022

Abstract

Freezing rain events have caused severe socioeconomic and ecosystem impacts. An understanding of how these events may evolve as the Earth warms is necessary to adequately adapt infrastructure to these changes. We present an analysis of projected changes to freezing rain events over North America relative to the 1980–2009 recent past climate for the periods during which +2, +3, and +4°C of global warming is attained. We diagnose freezing rain using four precipitation-type algorithms (Cantin and Bachand, Bourgouin, Ramer, and Baldwin) applied to four simulations of the fifth-generation Canadian Regional Climate Model (CRCM5) driven by four global climate models (GCMs). We find that the choice of driving GCM strongly influences the spatial pattern of projected change. The choice of algorithm has a comparatively smaller impact, and primarily affects the magnitude but not the sign of projected change. We identify several regions where all simulations and algorithms agree on the sign of change, with increases projected over portions of western Canada and decreases over the central, eastern, and southern United States. However, we also find large regions of disagreement on the sign of change depending on driving GCM and even ensemble member of the same GCM, highlighting the importance of examining freezing rain events in a multi-member ensemble of simulations driven by multiple GCMs to sufficiently account for uncertainty in projections of these hazardous events.

Plain Language Summary

Freezing rain events, or ice storms, can have major impacts on electrical infrastructure, agriculture, and road and air travel. Despite these impacts, relatively little research has been done on how these events may change as the Earth warms. We therefore examine several climate model simulations to determine how the frequency of freezing rain may change at different levels of future global warming. We focus in particular on how sensitive the projected changes are to the method used to identify freezing rain in the model output, as well as to the choice of climate model used to produce the projections. We find strong agreement among methods and models on a decrease in freezing rain frequency over much of the United States (from Texas northeastward to Maine) and an increase in freezing rain frequency over portions of western Canada (Alberta, Saskatchewan, Manitoba). In many other areas, however, the different methods and simulations disagree on the direction of projected change. Our findings highlight the importance of using many different climate models, rather than single simulations, to paint a clearer picture of the level of certainty in projections of freezing rain in the context of global warming.

1. Introduction

Freezing rain can have broad-ranging societal, economic and ecosystem impacts, ranging from hazardous conditions for air and road travel to severe damage to trees and electrical infrastructure. North America has experienced several ice storms in recent decades resulting in substantial damage, in some cases exceeding $1 billion US (Changnon, 2003; DeGaetano, 2000). Compared with other high-impact hazards, confidence in projected changes to ice storms as the climate changes remains low (IPCC, 2021). The challenge in understanding these changes stems in part from the conditions necessary for freezing rain formation, namely the coexistence of a warm layer of >0°C air aloft in which snowflakes melt and a sub-freezing cold layer at the surface that allows raindrops to freeze on contact (e.g., Brooks, 1920; Meisinger, 1920). Changes to freezing rain resulting from climate change thus depend on changes in conditions both at the surface and aloft.

Several techniques have been employed to examine the possible evolution of freezing rain events with climate change. The earliest studies on the topic analyzed output from global climate models (GCMs). Cheng et al. (2007) statistically downscaled four GCMs over Ontario, Canada, while Cheng et al. (2011) expanded this analysis using eight GCMs over a broader region of eastern Canada. Lambert and Hansen (2011) identified freezing rain directly from the output of a GCM (CGCM3, Scinocca et al., 2008). Klima and Morgan (2015) performed a thought experiment, applying a range of possible temperature changes to observed vertical temperature profiles of freezing rain over the eastern United States and Canada and examining how these changes may impact the precipitation type at the surface. Though regional details varied, these early studies generally agreed on a projected poleward shift in the region of most frequent freezing rain as the climate warms, with increasing freezing rain frequency to the north (e.g., portions of eastern Canada) and decreasing frequency to the south (e.g., the southern United States).

More recently, the improved spatial and temporal resolution permitted by dynamical downscaling using regional climate models (RCMs) have allowed for a more realistic representation of the observed freezing rain climatology (Bresson et al., 2017; St-Pierre et al., 2019). Jeong et al. (2018) explored projected changes to ice loads using the fifth-generation Canadian Regional Climate Model (CRCM5) (Martynov et al., 2013; Šeparović et al., 2013) at 0.44° horizontal resolution, driven by MPI-ESM and CanESM2 (Arora et al., 2011) under the RCP 4.5 and 8.5 forcing scenarios. They found that by the end of the 21st century, freezing rain frequency and amount is projected to decrease over much of the eastern United States but increase over parts of eastern Canada, with the largest changes in the CanESM2-driven RCP 8.5 simulation and the smallest changes with the MPI-ESM-driven RCP 4.5 simulation. Jeong et al. (2019) analyzed an ensemble of CanRCM4 (Scinocca et al., 2016) simulations driven by 50 CanESM2 (Arora et al., 2011) members with randomly perturbed initial conditions under RCP 8.5 forcing. They found similar results to Jeong et al. (2018), with decreasing freezing rain frequency over the contiguous United States and increasing frequency over Canada, with the largest increases occurring over western Canada. Matte et al. (2018) explored mixed precipitation (freezing rain and ice pellets) events using a 0.11° simulation of CRCM5 driven by MPI-ESM-LR centered on southern Québec, Canada. Their projections show a decrease in freezing rain frequency over most of their study domain (primarily southern Québec, New York, and New England) by the end of the century.

Though no study has yet compared output from multiple RCMs over North America, Kämäräinen et al. (2018) presented changes to freezing rain over Europe from six-hourly output of 3 RCMs driven by 7 GCMs from the European component of the Coordinated Regional Downscaling Experiment (EURO-CORDEX, Jacob et al., 2014). Kämäräinen et al. (2018) found large differences between the freezing rain climatologies simulated from the various RCM-GCM combinations due to differences in simulated surface and upper-air temperatures and precipitation frequency among the simulations. They found general agreement on a northward shift in the freezing rain climatology over Europe as the climate warms, with increasing frequency projected over northern and northeastern Europe and decreasing frequency over central and southeastern Europe.

Overall, the aforementioned dynamical downscaling experiments continue to agree on the projected poleward shift in North American freezing rain frequency found in earlier work. However, several sources of uncertainty remain to be quantified in these projections. First, only Jeong et al. (2018) used simulations driven by more than one driving GCM over the North American domain and found substantial regional differences between them, noting the need to increase the number of members to better evaluate model uncertainty. Given the importance of model response uncertainty on decadal time scales (Hawkins & Sutton, 2009; Lehner et al., 2020), an understanding of the range of projections associated with different models is important to appropriately plan future adaptation measures. Additionally, existing studies have typically chosen one precipitation-type algorithm to identify freezing rain in model output. For example, Lambert and Hansen (2011) used the Ramer (1993) method, while Jeong et al. (2018); Jeong et al. (2019) used the Bourgouin (2000) scheme. Only Matte et al. (2018) applied multiple algorithms (Baldwin & Contorno, 1993; Bourgouin, 2000; Cantin & Bachand, 1993; Czys et al., 1996; Ramer, 1993) over their relatively small domain. They found a large variation in the mean annual hours of mixed precipitation identified using the different algorithms for the recent past climate, with Czys identifying the least and Baldwin the most.

Over North America, McCray, Thériault, et al. (2022) applied four precipitation-type algorithms (Baldwin & Contorno, 1993; Bourgouin, 2000; Cantin & Bachand, 1993; Ramer, 1993) to the output of CRCM5 simulations driven by ERA-Interim and four GCMs for the recent past climate (1980–2009). They compared the results obtained using the different algorithms and found that while each algorithm was able to reproduce the spatial pattern of the observed freezing rain climatology, there were substantial differences in freezing rain frequency depending on algorithm chosen and even on selections made for parameters within individual algorithms. In particular, the Ramer algorithm overestimated freezing rain frequency, while Cantin and Bachand tended to

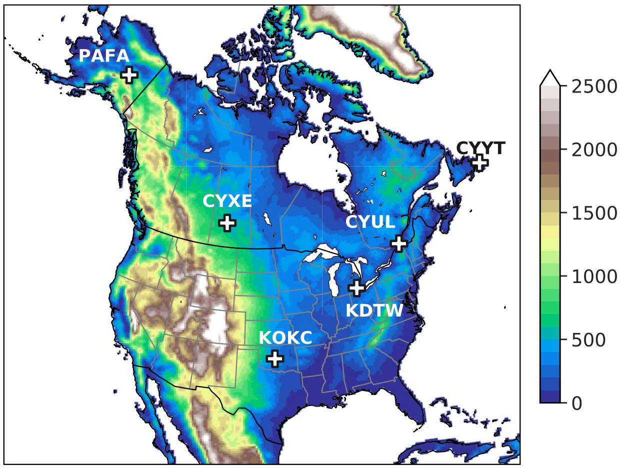

Figure 1. Model topography over the fifth-generation Canadian Regional Climate Model (CRCM5) domain studied here. Individual stations described in the text are indicated: PAFA (Anchorage, Alaska), CYXE (Saskatoon, Saskatchewan), KOKC (Oklahoma City, Oklahoma), KDTW (Detroit, Michigan), CYUL (Montréal, Québec), and CYYT (Saint John's, Newfoundland).

underestimate it. McCray, Thériault, et al. (2022) also demonstrated that the choice of driving GCM had a large impact on the spatial pattern of annual hours of freezing rain for the recent past climate. For example, the CRCM5 driven by GFDL-ESM2M produced much more frequent freezing rain over southern United States, in particular Oklahoma and Texas, compared with the other simulations and observations.

The purpose of this study is to expand on the analysis presented in McCray, Thériault, et al. (2022) to examine projected changes to freezing rain frequency in the future climate using a suite of CRCM5 simulations driven by four GCMs. We explore the impact of precipitation-type algorithm selection on these projected changes as well as the variability associated with the choice of driving GCM. Finally, we explore five simulations driven by a single GCM to place our findings in the context of natural variability. This work aims to provide a more complete understanding of the range of possible changes to the freezing rain climatology in the context of a warming climate, and to provide a clearer picture of the level of uncertainty associated with these projections.

2. Materials and Methods

2.1. Climate Simulations

The simulations and precipitation-type algorithms used here are the same as those presented in McCray, Thériault, et al. (2022). We identify the frequency of freezing rain in a suite of CRCM5 simulations at 0.22° horizontal resolution (Figure 1). We analyze output from a suite of simulations driven by models within the Coupled Model Intercomparison Project Phase 5 (CMIP5), including the second generation Canadian Earth System Model (CanESM2) (Arora et al., 2011), the low-resolution version of the Max Planck Institute Earth System Model (MPI-ESM-LR) (Giorgetta et al., 2013), the Geophysical Fluid Dynamics Laboratory Earth System Model version 2 (GFDL-ESM2M) (Dunne et al., 2012), and the Centre National de Recherches Météorologiques climate model version 5 (CNRM-CM5) (Voldoire et al., 2013) using observed greenhouse gas concentrations for 1950–2005 and following the RCP 8.5 emissions scenario for 2006–2100. We also use four additional CanESM2-driven simulations with randomly perturbed initial conditions to gain insight into the magnitude of natural variability in the projections.

Simulations are run on 56 hybrid levels with a 10-min time step, with data archived every three hours at the surface and 17 (CRCM5 driven by MPI-ESM-LR), 22 (CanESM2), or 27 (GFDL-ESM2M and CNRM-CM5) pressure levels. The 27-level simulations only add additional stratospheric levels (≤70 hPa) which do not impact freezing rain identification, while the MPI-ESM-LR-driven simulation lack near-surface levels (960, 970, 980, 985 and 990 hPa) in addition to the 950-, 975-, and 1000-hPa level data available from the other simulations. Sensitivity tests (not shown) demonstrate that the effect of these additional levels have a negligible impact on the simulated freezing rain climatology. For a complete description of the CRCM5 and its parameterizations, see Section 2a in St-Pierre et al. (2019).

2.2. Precipitation-Type Algorithms

We apply the four precipitation-type algorithms of varying complexity described in McCray, Thériault, et al. (2022) to model output. The simplest method devised by Cantin and Bachand (1993) uses the thicknesses of the 1000–850-hPa and 850–700-hPa layers as proxies for the near-surface cold (<0°C) and warm (>0°C) layers, respectively. Precipitation type is determined based on thresholds for each layer. The Bourgouin (2000) method calculates the positive (>0°C) and negative (<0°C) areas on the thermodynamic diagram between 0°C and the dry-bulb temperature, with thresholds related to each distinguishing the different precipitation types (rain, snow, ice pellets, freezing rain, or mixtures).

Unlike Cantin and Bachand and Bourgouin, the Ramer (1993) and Baldwin and Contorno (1993) methods begin by identifying the level at which precipitation forms based on different saturation criteria. This allows

Table 1
30-Year Periods During Which Each Global Warming Level Is Reached for the Given Driving Global Climate Model Under the RCP 8.5 Forcing Scenario

	+2°C	+3°C	+4°C
GFDL-ESM2M	2038–2067	2067–2096	–
CNRM-CM5	2030–2059	2053–2082	–
MPI-ESM-LR	2022–2051	2047–2076	2067–2096
CanESM2 (r1i1p1)	2013–2042	2035–2064	2054–2083
CanESM2 (r2i1p1)	2012–2041	2034–2063	2052–2081
CanESM2 (r3i1p1)	2013–2042	2035–2064	2054–2083
CanESM2 (r4i1p1)	2012–2041	2033–2062	2053–2082
CanESM2 (r5i1p1)	2011–2040	2033–2062	2053–2082

for identification of freezing precipitation formed through the supercooled warm rain process (Bocchieri, 1980; Huffman & Norman, 1988; Rauber et al., 2000) which cannot be detected using Cantin and Bachand or Bourgouin. In this process, precipitation initially forms as liquid drops within shallow near-surface saturated layers with temperatures too warm for heterogeneous ice nucleation (warmer than approximately −10°C). Given the shallowness of these layers, this process often produces freezing drizzle, but may also produce freezing rain (Rauber et al., 2000).

The Ramer method calculates the change in ice fraction of the hydrometeors as they fall from the precipitation generation level toward the surface, with surface precipitation type dependent on ice fraction and surface temperature. Baldwin instead compares the areas (layer depth times layer-mean wet-bulb temperature) of different layers, with thresholds for these layer areas determining the surface precipitation phase. While Bourgouin uses dry-bulb temperature, Ramer and Baldwin use wet-bulb temperature profiles allowing for consideration of evaporative cooling. We use a 90% relative humidity threshold for saturation with Ramer, with a dewpoint depression <6°C threshold for Baldwin. Sensitivity tests for these thresholds and additional detail on the algorithms can be found in Section 2c of McCray, Thériault, et al. (2022).

We require precipitation rate to be at least 1 mm d^{-1} before applying algorithms as the CRCM5, like other RCMs, tends to overestimate the frequency of very light precipitation. This threshold was also used in previous CRCM5 studies of freezing precipitation (Bresson et al., 2017; Matte et al., 2018; McCray, Thériault, et al. (2022); St-Pierre et al., 2019).

2.3. Global Warming Levels

The driving GCMs used here have a broad range of equilibrium climate sensitivities, ranging from 2.5 K for MPI-ESM-LR to 3.7 K for CanESM2 (Andrews et al., 2012). The level of global warming at the end of the century therefore varies substantially depending on driving GCM. We examine changes relative to the change in global mean surface temperature, rather than relative to fixed periods (e.g., 2070–2099). We follow the method of Nikulin et al. (2018) to identify global warming level (GWL) periods, calculated relative to the 1850–1900 baseline period, representative of the pre-industrial global mean temperature. For each of the four GCMs, we calculate the annual mean global mean surface temperature and subtract the 1850–1900 mean from this value. We then calculate the centered 30-year moving average ($n - 14$, $n + 15$) of the anomaly. The first period during which the moving average exceeds a given GWL is identified as the GWL period for that level.

We present results at three GWLs: +2°C, +3°C, and +4°C. Lower levels (e.g., +1.5°C) are attained very early in some GCMs with higher climate sensitivity (e.g., 1999–2028 for CanESM2) which leads to a sometimes large overlap with our 1980–2009 reference period for the freezing rain climatology. The +4°C period is only attained before 2100 (the end of our simulations) for the two warmest GCMs, MPI-ESM-LR and CanESM2 (Table 1). While we present results for simulations forced with the RCP 8.5 emissions scenario, the RCP 4.5 scenario simulations produce very similar results for a given driving GCM and GWL. However only one driving GCM (CanESM2) reaches +3°C, and none reach +4°C, under RCP 4.5. For reference, IPCC (2021) assessed +2°C as very likely to be reached in the mid-term period (2041–2060) for all five Shared Socio-economic Pathway (SSP) scenarios they presented. In the long term (2081–2100), global warming of +3°C is within the very likely range for four of the five SSPs (all except SSP1-1.9), while +4°C is very likely for the two warmest scenarios (SSP3-7.0 and SSP5-8.5) (IPCC, 2021).

3. Projected Changes to Freezing Rain Frequency

3.1. Effect of Driving GCM on Projected Changes

McCray, Thériault, et al. (2022) demonstrated that the CRCM5 driven by both ERA-Interim reanalysis and the four GCMs was able to reasonably reproduce the North American climatology of freezing rain. However, they

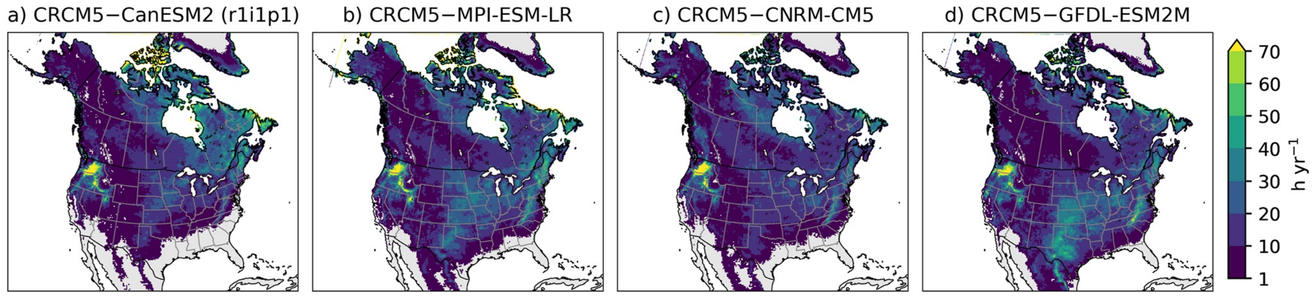

Figure 2. Multi-algorithm mean of the median annual hours of freezing rain for the 1980–2009 reference period for the fifth-generation Canadian Regional Climate Model driven by (a) second generation Canadian Earth System Model, (b) low-resolution version of the Max Planck Institute Earth System Model (MPI-ESM-LR), (c) Centre National de Recherches Météorologiques climate model version 5 (CNRM-CM5), and (d) Geophysical Fluid Dynamics Laboratory Earth System Model version 2 (GFDL-ESM2M).

found sometimes substantial differences in the resultant climatology depending on driving GCM. Among the four simulations for the recent past climate (1980–2009), CRCM5–CanESM2 produces an axis of most-frequent freezing rain situated furthest to the north (Figure 2a), while the CRCM5–GFDL-ESM2M simulation produces the most freezing rain over the southern United States (Figure 2d). McCray, Thériault, et al. (2022) found that the CRCM5–MPI-ESM-LR simulation produced a freezing rain climatology that was best correlated with observations while the CRCM5–GFDL-ESM2M had the weakest correlations (see their Table 3), though some simulations were better than others over particular regions. A complete evaluation of the ability of the CRCM5 to reproduce the recent past climatology of freezing rain can be found in McCray, Thériault, et al. (2022).

We now analyze the mean change in the median annual hours of freezing rain among the four algorithms for each combination of simulation and GWL to determine the impact of driving GCM on projected changes. At all levels of global warming, each simulation shows a northwestward shift in the region of frequent freezing rain, with decreases in freezing rain frequency over the southern, central, and eastern United States and increases to the north, particularly over the Canadian Prairies (Figure 3). This spatial pattern is consistent with that found by Jeong et al. (2019) for projected changes to ice thicknesses in the CanRCM4 driven by CanESM2.

The dominant signal at the +2°C GWL is the decrease in freezing rain frequency over the eastern United States, though the CanESM2- and CNRM-CM5-driven simulations also show coherent increases over portions of western and central Canada (Figures 3a and 3g). The pattern of change over Canada is noisier in the MPI-ESM-LR- and GFDL-ESM2M-driven simulations (Figures 3d and 3i).

At +3°C of global warming, a strong signal of increasing freezing rain frequency emerges over much of western and central Canada, with an additional region of projected increase over Alaska particularly for the MPI-ESM-LR-driven simulation (Figure 3e). Projected decreases over the United States strengthen in magnitude and expand slightly. For the CanESM2- and MPI-ESM-LR-driven simulations that reach +4°C of global warming, projected increases and decreases strengthen in magnitude at this level though the geographic extent of projected change expands only slightly compared to the +3°C GWL (Figures 3c and 3f).

We focus on three individual stations to illustrate differences among the four simulations: Saskatoon, Saskatchewan (CYXE), located within the region of coherent projected increase over western Canada; Montréal, Québec (CYUL), positioned in a region of greater uncertainty on the sign of change; and Oklahoma City, Oklahoma (KOKC), within the region of coherent projected decrease over the U.S. Great Plains (Figure 4). At CYXE, only the CNRM-CM5- and GFDL-ESM2M-driven simulations project an increase at the +2°C GWL, but all four simulations show an increase in freezing rain frequency at +3°C of global warming (Figure 4a). The GFDL-ESM2M-driven simulation produces the least freezing rain at CYXE in the past climate, but the relative future changes are comparable to the other simulations.

Unlike at CYXE, each simulation produces a different trend at CYUL (Figure 4b). The CanESM2-driven simulation shows a strong decrease at +2°C that remains stable at +3°C before decreasing further at +4°C. The CNRM-CM5-driven simulation shows a near-constant trend at +2 and + 3°C. CRCM5 driven by MPI-ESM-LR has a decrease in freezing rain frequency at +2°C, but no substantial changes at +3 or +4°C. Median freezing

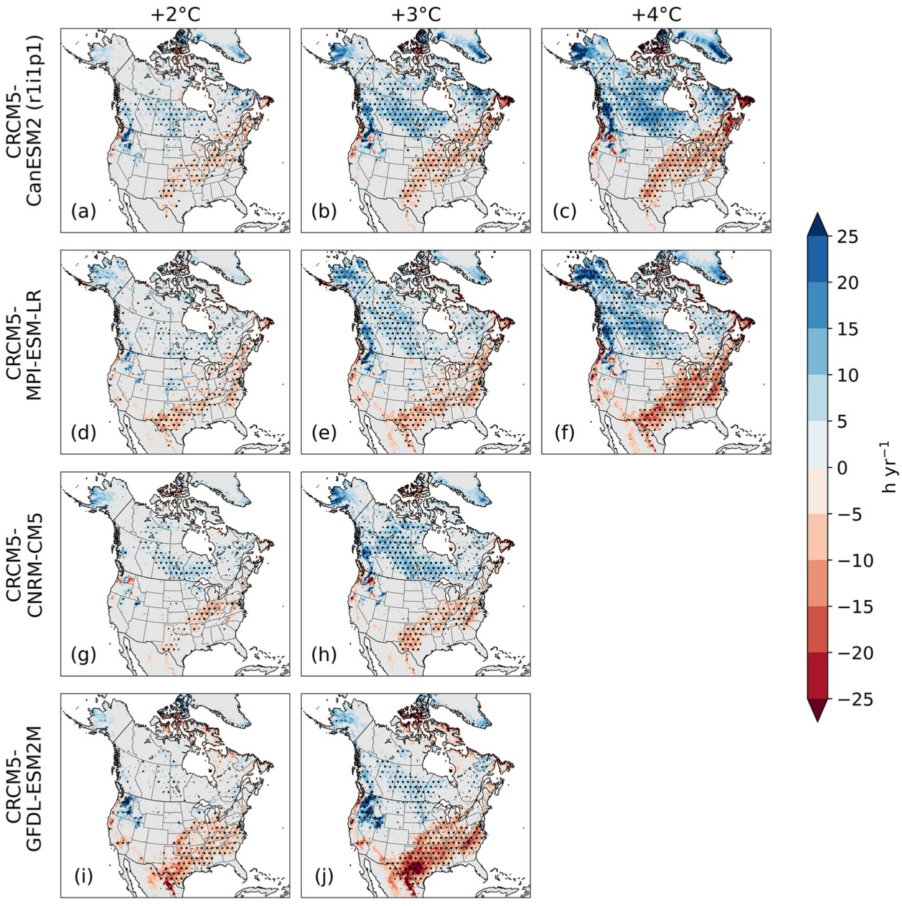

Figure 3. Multi-algorithm mean of the change in frequency of freezing rain at each grid point between the (a, d, g and i) +2°C, (b, e, h and j) +3°C, and (c and f) +4°C global warming level periods and 1980–2009 for the fifth-generation Canadian Regional Climate Model (CRCM5) driven by (a–c) CanESM2, (d–f) MPI-ESM-LR, (g and h) CNRM-CM5, and (i and j) GFDL-ESM2M. Changes of magnitude <5 hr yr^{-1} are not plotted. Stippling indicates grid points where the four algorithms agree on the sign of the change.

rain frequencies decrease for each degree of warming in the GFDL-ESM2M-driven simulation, however the interquartile range of values at +2°C remains within the range for the recent past climate.

At KOKC, all four simulations show a clear decreasing trend at each GWL with the exception of the CanESM2-driven simulation that has a slight increase in the median and extreme values at +4°C relative to +3°C (Figure 4c). Additionally, the MPI-ESM-LR and GFDL-ESM2M simulations have several extreme (exceeding the 95th percentile) values that exceed those of the past climate and +2°C, suggesting a potential transient increase in years with more frequent freezing rain.

3.2. Effect of Algorithm Selection on Projected Changes

We next examine the impact of algorithm selection on projected changes. Regions with substantial mean changes (magnitude ≥5 hr yr^{-1}) in Figure 3 are generally stippled, indicating overall agreement on the sign of change among the different algorithms. To illustrate differences between algorithms, we focus on a single simulation-GWL combination, the CRCM5 driven by CanESM2 member r1i1p1 at +3°C. McCray, Thériault, et al. (2022) demonstrated that the Cantin and Bachand method generally identified the least freezing rain while Ramer identified the most among the four algorithms for the recent past climate. Consequently, the magnitudes of projected changes are smallest for Cantin and Bachand (Figure 5a) and largest for Ramer (Figure 5c). The spatial pattern of the change is very similar among algorithms with the exception of Cantin and Bachand, which

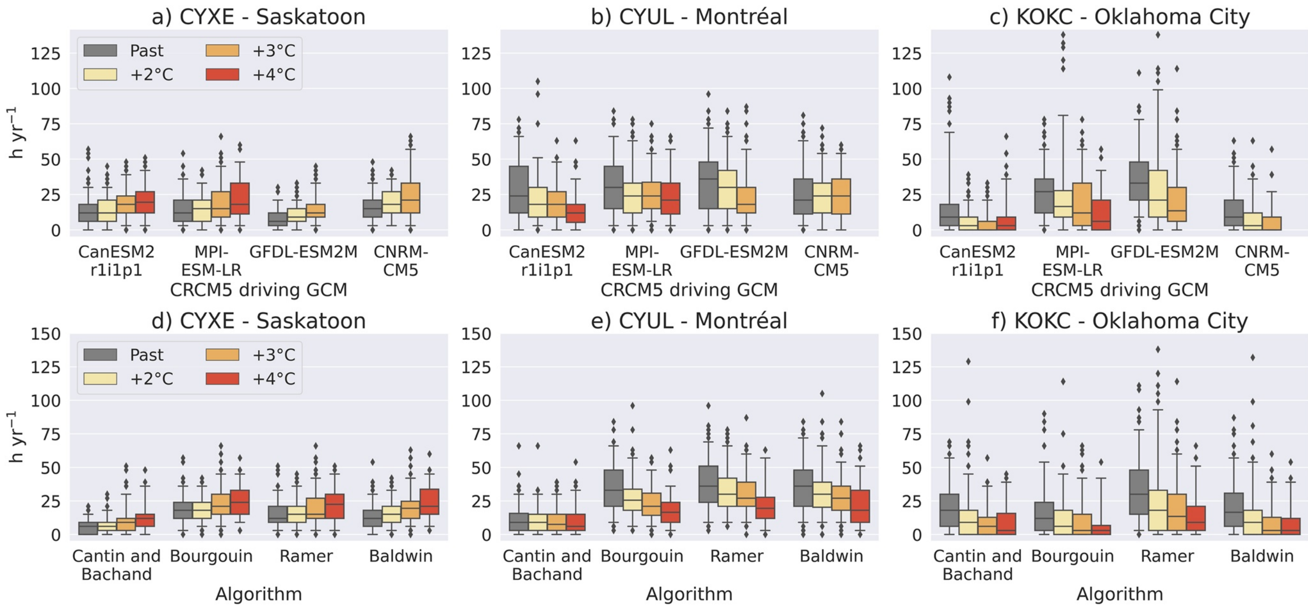

Figure 4. Box plots displaying the range of annual hours of freezing rain simulated for four 30-year periods: The recent past climate (1980–2009, gray) and the 30-year period surrounding the +2°C (yellow), +3°C (orange), and +4°C (red) global warming levels for (top row) results from the four algorithms grouped by global climate model (GCM) used to drive the CRCM5 and (bottom row) results for the four simulations grouped by precipitation-type algorithm at (a, d) CYXE, (b, e) CYUL, and (c, f) KOKC. Boxes indicate the interquartile range, with the horizontal line indicating the median value. Whiskers extend to the 5th and 95th percentiles, with values outside these ranges plotted as diamonds.

shows virtually no change over northern Canada and Alaska, regions where the other three methods show large increases in some regions.

Differences displayed relative to their initial frequency of freezing rain for the past climate (Figures 5e–5h) are more similar than absolute differences. Baldwin shows the largest relative increase in freezing rain frequency over western Canada (Figure 5h), while Cantin and Bachand identifies a median of 0 hr yr^{-1} over much of this region in both the past and future climates (Figures 5a and 5e). The similarity between spatial patterns among the algorithms for a given simulation is much greater than that between simulations driven by different GCMs (Figure 3). Choice of algorithm does not therefore appear to have a substantial impact on the spatial pattern of change.

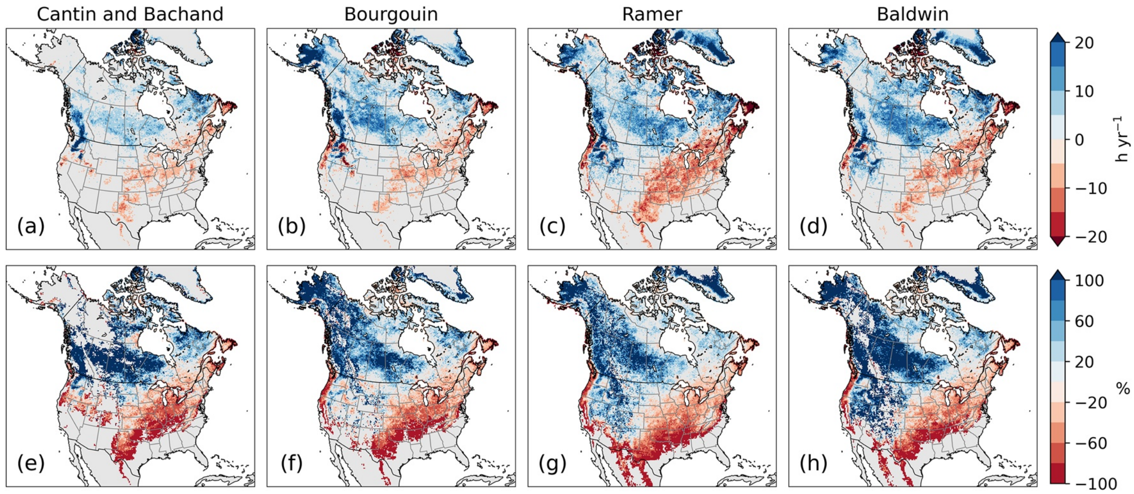

Figure 5. (a–d) Projected absolute and (e–h) relative change in the median annual hours of freezing rain at the time of +3°C (2035–2064) relative to 1980–2009 for the CRCM5 driven by CanESM2 member r1i1p1 calculated using the Cantin and Bachand (a, e), Bourgouin (b and f), Ramer (c and g) and Baldwin (d and h) algorithms. Changes of magnitude ≥5 hr yr^{-1} or 20% are plotted.

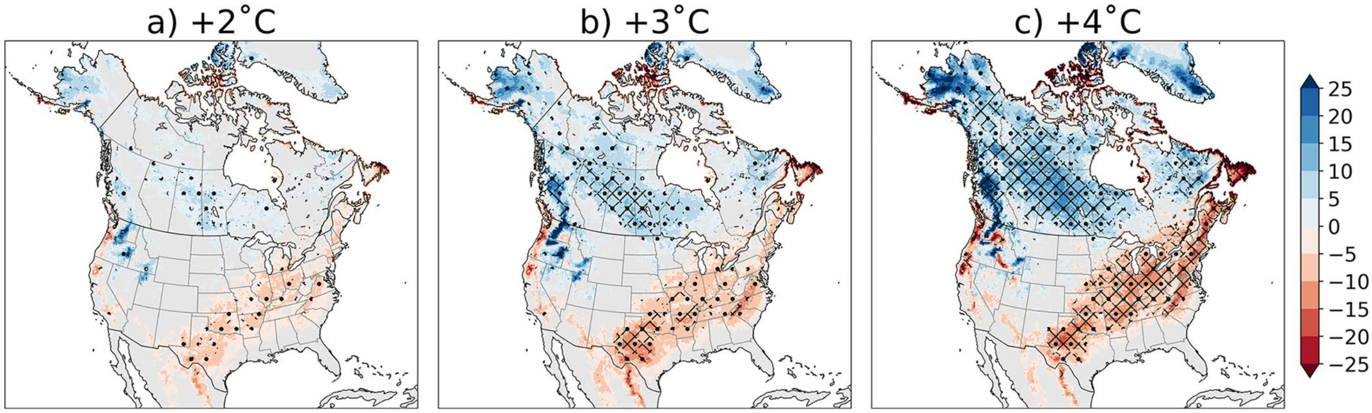

Figure 6. Multi-algorithm, multi-simulation mean of the change in median annual hours of freezing rain at each global warming level relative to the 1980–2009 median. Stippling indicates grid points where 80% of combinations agree on the sign of change, while hatching indicates regions where 100% of combinations agree. Calculations include a total of 16 combinations (4 simulations x 4 algorithms) for (a) +2°C and (b) +3°C, and (c) 8 combinations (2 simulations x 4 algorithms) for +4°C.

Similarly, the box plots for changes at the three cities grouped by algorithm (Figure 4) generally show much less variation than those between driving GCM (Figure 4). At CYXE (Figure 4d), each algorithm (including values from all four simulations) shows a clear increasing trend especially after the +2°C GWL. While different algorithms produce different initial frequencies of freezing rain, the qualitative trend is generally the same for each. At CYUL (Figure 4e), the Bourgouin, Ramer, and Baldwin algorithms produce a strong decreasing trend. Cantin and Bachand, however, has much less freezing rain in the past climate and also shows no trend at any of the three levels. Matte et al. (2018) noted the inability of the Cantin and Bachand method to detect the local maximum in freezing rain frequency in the St. Lawrence River Valley, including at CYUL, and attributed this to this method's use of layer thicknesses rather than detailed low-level temperature profile information necessary to identify shallow cold layers in the valley.

At KOKC, all algorithms generally agree on the decreasing trend for each GWL (Figure 4f). Ramer produces the most freezing rain, though unlike at the other locations Bourgouin, and not Cantin and Bachand, produces the least for the recent past climate. All four algorithms show a decrease at +2°C, though several extreme values greater than those obtained for the recent past climate appear, as in Figure 4.

3.3. Combined Uncertainty

We now combine the preceding analyses and explore the extent to which the combinations of precipitation-type algorithm and simulations driven by different GCMs agree on the sign of projected change, allowing us to highlight regions of robust projected increases/decrease and those where uncertainty is greatest (Figure 6). At +2°C, very few regions exhibit strong agreement on the sign of change (Figure 6a). The largest region with agreement is the reduction in freezing rain frequency from Texas northeastward to Ohio, roughly the southern half of the region that currently sees freezing rain most frequently (e.g., Cortinas et al., 2004; McCray et al., 2019). The most coherent region of projected increase in freezing rain frequency is over the Canadian Prairie provinces, from northern Alberta southeastward to Saskatchewan and Manitoba. Additional smaller regions of agreement on change are the increasing trend over the complex terrain of Washington, Oregon, and Idaho and decreases along the eastern coast of Newfoundland, where freezing rain is observed most frequently in the current climate (Cortinas et al., 2004; McCray et al., 2019). Very few grid points exhibit 100% agreement among all simulation-algorithm combinations.

At +3°C, the regions of 80% and 100% agreement on the sign of change expand substantially (Figure 6b). All simulations and algorithms agree on large decreases in freezing rain frequency over much of Texas northeastward to Kentucky. The spatial extent of the region of increasing freezing rain frequency expands substantially northward at +3°C. All combinations agree on an increase in freezing rain frequency over northern Alberta southeastward into northern Ontario. Regions of 80% agreement also emerge northward and westward into the Canadian Rockies of British Columbia, portions of the Canadian territories, and Alaska. In eastern Canada, a

10.1029/2022JD036935

Table 2
Median Annual Hours of Freezing Rain at Selected Cities Among the Four Algorithms and Four Simulations (Two for the +4°C Global Warming Level) for Four 30-Year Periods: The 1980–2009 Recent Past Climate and the +2°C, +3°C, and +4°C GWL Periods

	1980–2009	+2°C	+3°C	+4°C
Fairbanks, Alaska (PAFA)	3 (0–24)	6 (0–39)	12 (0–48)	15 (0–60)
Saskatoon, Saskatchewan (CYXE)	12 (0–33)	12 (0–33)	15 (3–42)	18 (3–45)
Saint John's, Newfoundland (CYYT)	27 (0–114)	6 (0–60)	0 (0–27)	0 (0–12)
Montréal, Québec (CYUL)	27 (3–66)	24 (3–60)	21 (0–51)	15 (0–48)
Oklahoma City, Oklahoma (KOKC)	18 (0–63)	9 (0–60)	6 (0–42)	3 (0–42)
Detroit, Michigan (KDTW)	21 (3–60)	18 (3–45)	15 (0–42)	9 (0–33)

Note. Values in parentheses indicate the 5th–95th percentiles of annual values. Station locations are indicated in Figure 1.

region of 80% agreement on increasing freezing rain frequency also emerges over Labrador and surrounding portions of Québec.

Finally, the magnitude and level of agreement on changes at +4°C increase substantially (Figure 6c), with 100% agreement on the sign of change over most regions with plotted changes. However, caution must be taken when examining these results, as only the simulations driven by the two warmest driving GCMs (CanESM2 and MPI-ESM-LR) attain +4°C by 2100, and these calculations are based on eight combinations rather than 16.

We summarize results for selected cities, including both the median and extreme values for the various periods, in Table 2. At Detroit and Saint John's, median freezing rain frequency and extremes decline substantially. Saint John's, the location that currently observes the most freezing rain, is projected to observe a rapid decline in freezing rain frequency from a median of 27 hr yr^{-1} to 6 hr yr^{-1} at +2°C and 0 hr yr^{-1} at +3°C of global warming, as surface temperatures warm quickly at this coastal location. The current climate 95th percentile of 114 hr yr^{-1} decreases to just 27 hr yr^{-1}, equivalent to the 1980–2009 median value, at +3°C of warming.

At CYUL and KOKC, a clear decreasing trend emerges in the medians, though the 95th percentile values remain relatively high even at +4°C of warming, decreasing from 66 (63) to 48 (42) h yr^{-1} at CYUL (KOKC). This suggests the need for additional analysis of extremes, as extreme events may still occur (or even increase in frequency) even if the median annual frequency declines.

At Fairbanks, while the medians increase steadily, the 95th percentiles increase rapidly, more than doubling from 24 hr yr^{-1} for the recent past climate to 60 hr yr^{-1} at +4°C. Uncertainty in projections over Alaska is partly related to the absence of freezing rain there when using Cantin and Bachand (Figure 5a). Finally, at CYXE, both the median and 5th–95th percentile ranges are unchanged at +2°C, but begin to slowly increase at +3°C.

3.4. Natural Variability

Jeong et al. (2019), using a 50-member initial-condition ensemble of CanRCM4 driven by CanESM2, found large natural variability in their metric for changes to extreme freezing rain (the 50-year return level of annual maximum ice thickness). The 5th and 95th percentiles of change among ensemble members displayed changes of differing sign over many regions (see their Figure 5). In addition to the four simulations we explored previously, four additional CRCM5 simulations driven by different CanESM2 ensemble members are available. Despite the small sample size, these five CanESM2-driven simulations allow us to examine the degree of projected changes to our freezing rain metric (median annual hours) relative to natural variability.

As we only have five CRCM5–CanESM2 members, we explore the differences between the maximum and minimum projected change at each grid point among the members (Figure 7). Consistent with Jeong et al. (2019), the sign of the ensemble maximum and minimum values varies over many regions. This is the case in particular at the +2°C GWL (Figures 7a–7c), with differing signs over much of northern Canada and Alaska, Québec and Ontario, the U.S. northern Plains and the Rocky Mountains. The region of disagreement on the sign of change narrows at +3°C (Figures 7d–7f), though uncertainty remains over much of southern and central Québec, for example, By +4°C of global warming (Figures 7g–7i) the region of uncertainty on the sign of change narrows

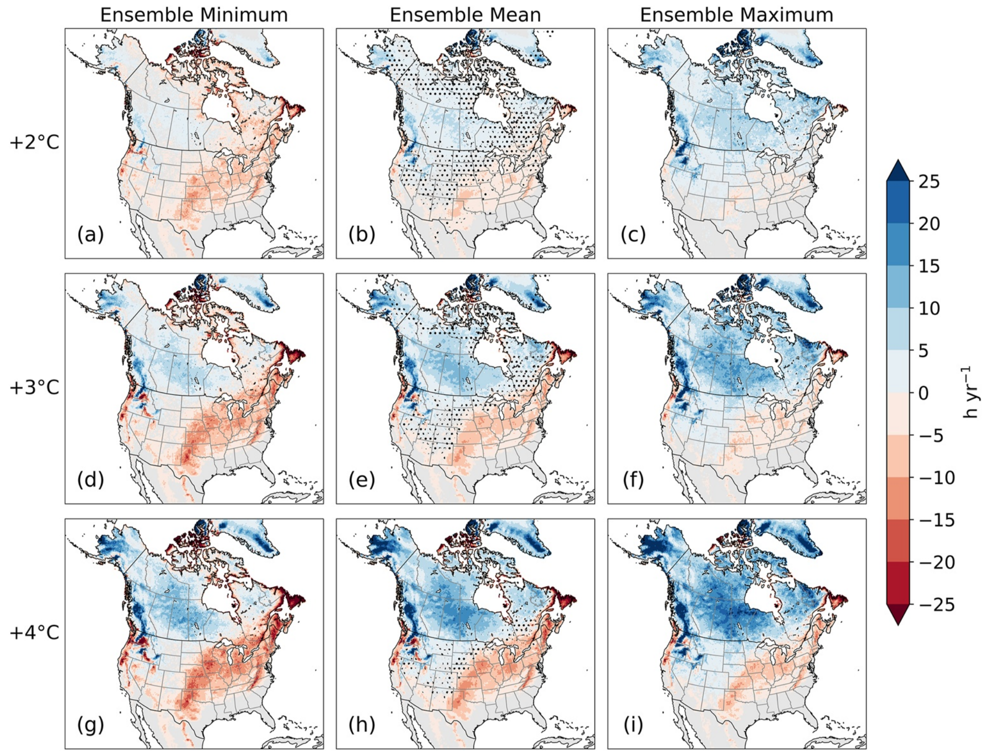

Figure 7. Minimum (left column), mean (center), and maximum (right column) of the multi-algorithm mean change in the median annual hours of freezing rain for the CRCM5 driven by five members of the CanESM2 ensemble members from 1980 to 2009 to each global warming level: (a–c) +2°C, (d–f) +3°C, and (g–i) +4°C. Stippling in the center column indicates grid points where the ensemble minimum and maximum differ on the sign of projected change.

considerably, though a band of disagreement persists at the border of mean increase/decrease from New Mexico northeastward to central Québec. The uncertainty among our ensemble is generally lower than that presented by Jeong et al. (2019), likely a result of our use of a smaller ensemble and also because we are examining changes in the frequency of freezing rain rather than changes to the annual extreme ice accretion.

At the individual station level, though differences between CRCM5 driven by the different CanESM2 members are much smaller than differences between simulations driven by different GCMs (Figure 4), differences in trends are apparent at some stations and GWLs (Figure 8). At CYXE (Figure 8a), CRCM5 driven by CanESM2 member r5i1p1 projects an increase in the median from the recent past climate to +2°C, but little change at +3°C and +4°C. Simulations driven by members r1i1p1 and r3i1p1 show little change at +2°C but an increase for the two warmer levels, while the remaining two members suggest a clearer increasing trend at each degree of warming. At CYUL, members r3i1p1 and r5i1p1 show a strong decreasing trend for each degree of warming, while r4i1p1 suggests little change at +2°C (Figure 8b). The signal is noisier at KOKC (Figure 8c), though most members tend

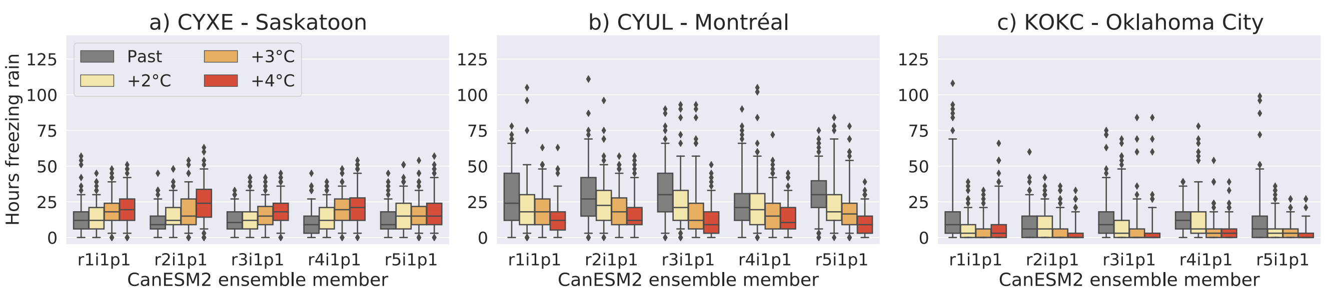

Figure 8. Box plots as in Figure 4 but displaying the range of annual hours of freezing rain observed for four 30-year periods for the five CanESM2-driven CRCM5 simulations at (a) Saskatoon, Saskatchewan (CYXE), (b) Montréal, Québec (CYUL), and (c) Oklahoma City, Oklahoma (KOKC).

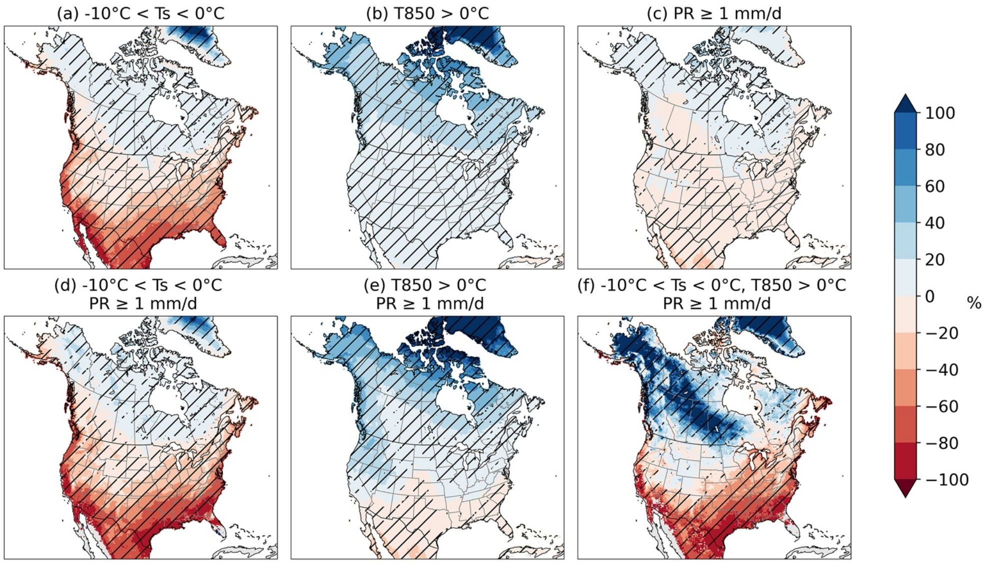

Figure 9. Mean projected relative changes in the annual frequency of several ingredients for freezing rain at +3°C of global warming relative to the 1980–2009 mean frequency among the four CRCM5 simulations driven by different global models discussed here, including (a) 2-m temperature Ts between −10 and 0°C, (b) 850-hPa temperature >0°C, (c) precipitation rate ≥1 mm d^{-1}, (d) the coincidence of −10°C < Ts < 0°C with precipitation rate ≥1 mm d^{-1}, (e) the coincidence of 850-hPa temperature >0°C with precipitation rate ≥1 mm d^{-1}, and (f) the combined occurrence of all three conditions. Hatching indicates grid points where the four simulations agree on the sign of the change.

to agree on an overall decreasing trend. Little change is projected for some members, for example, r5i1p1 from +2°C to +3°C and r4i1p1 from +3°C to +4°C.

4. Discussion

The projected northwestward shift in the region of most frequent freezing rain in North America found here agrees with prior studies over this region, including Lambert and Hansen (2011) and Jeong et al. (2018); Jeong et al. (2019). Two key remaining questions are what physical processes lead to this shift and what is responsible for the regions of greater uncertainty. Lambert and Hansen (2011) suggested the reduced frequency of sub-freezing surface temperature over the United States combined with an increased frequency of strong cyclones advecting warm air further northward as possible mechanisms. Jeong et al. (2019) presented projected changes in the frequency of the thermodynamic ingredients for freezing rain, including surface temperature Ts between −10°C and 0°C, 850-hPa temperature T850 > 3°C, and the combination of Ts < 0°C and T850 > 3°C. Projected warming both at the surface and aloft led to a northwestward shift in the spatial pattern of this last measure that closely resembled the projected changes to freezing rain.

We perform a similar analysis to Jeong et al. (2019) and calculate the change in frequency of several ingredients for freezing rain. We focus on the frequency change of three variables for the +3°C GWL: −10°C < Ts < 0°C, T850 > 0°C, and the coincidence of the two conditions. Finally, we add our precipitation rate threshold PR ≥ 1 mm d^{-1} to each of the metrics to examine the frequency of these conditions during precipitation.

Among all simulations, the frequency of −10°C < Ts < 0°C is projected to increase over most of Canada and decrease over most of the contiguous United States at +3°C, with mean decreases of >60% for precipitation occurring with this temperature range (Figures 9a and 9d). As the surface warms, subfreezing surface temperatures become less frequent to the south but temperatures ≥−10°C become more frequent to the north.

The frequency of T850 > 0°C is projected to increase by >40% over northern Canada and slightly (0%–20%) over the contiguous United States, with stronger increases projected when the precipitation threshold is included (Figures 9b and 9e). The frequency of precipitation of at least 1 mm d^{-1} is projected to decrease slightly over much of the southern United States but increase slightly over northern Canada and Alaska (Figure 9c), leading to a slight decrease in the frequency of precipitation with T850 > 0°C to the south and an increase of >40% over much of northern Canada and Alaska (Figure 9e).

The combination of the three ingredients (Figure 9f) leads to a pattern closely resembling that of the projected changes to freezing rain frequency at the +3°C GWL (Figure 6b). The large reduction in freezing rain frequency over the southern United States is largely the result of surface warming, with subfreezing surface temperatures becoming less common. The projected increase in freezing rain over western Canada appears to primarily result from warming aloft as evidenced by the substantial increase in the frequency of T850 > 0°C. This increase is also partly related to warming at the surface. Though the frequency of Ts < 0°C is projected to decrease over most of Canada (not shown), the frequency of temperatures within the −10°C–0°C range is projected to increase slightly as the surface warms and very cold temperatures become less common. Surface temperatures will thus more frequently fall within the range conducive to freezing precipitation (Cortinas et al., 2004).

While we have focused on projected changes to the thermodynamic ingredients for freezing rain here, an important aspect that is beyond the scope of this paper is possible changes to the synoptic-dynamic patterns leading to freezing rain. As these patterns and the storm tracks associated with freezing rain vary regionally, additional region-specific studies are warranted that focus on these changes. Studies on synoptic patterns leading to freezing rain for the recent past climate (e.g., Rauber et al., 2001) may serve as starting points for this work, including Ressler et al. (2012) for Montréal, Kochtubajda et al. (2017) for western Canada, and McCray et al. (2021) for the south-central United States. For example, Mittermeier et al. (2021) applied a machine-learning technique to identify synoptic-scale pressure patterns associated with mixed precipitation (freezing rain and/or ice pellets) in Montréal in CRCM5 output for the recent passut climate based on the patterns identified in Ressler et al. (2012). Such an approach could be applied to the future climate to examine changes to the frequency and characteristics of these patterns.

5. Conclusions

Existing studies of freezing rain in the context of climate change over North America have relied on a single algorithm applied to a single GCM (Lambert & Hansen, 2011) or one to two GCMs downscaled by an RCM (Jeong et al., 2018, 2019), or multiple algorithms applied to a single GCM-RCM combination (Matte et al., 2018). Kämäräinen et al. (2018) applied a single algorithm to a matrix of several RCMs driven by several GCMs over Europe. Here, we have presented the first North American analysis of projected changes to freezing rain using multiple algorithms applied to an ensemble of simulations of an RCM driven by multiple GCMs. While the frequencies of freezing rain identified depend greatly on the algorithm as demonstrated by McCray, Thériault, et al. (2022), the spatial pattern of changes is generally very similar for a given simulation regardless of algorithm. An important outlier was the Cantin and Bachand method, the simplest method relying only on geopotential height on three levels.

While algorithm selection has a limited impact on projected changes to freezing rain events, the choice of driving GCM has a much larger effect, highlighting the necessity of examining simulations driven by multiple GCMs to develop a complete picture of the range of possible changes. Use of a single RCM-GCM combination may lead to overconfidence in a particular projected change in some regions. Several studies on freezing rain in climate models have focused on southern Québec given the frequency of severe freezing rain events in the Saint Lawrence River Valley. For example, Matte et al. (2018) found a decreasing trend in mixed precipitation events over southern Québec in their CRCM5 simulation driven by MPI-ESM-LR. Our results highlight the uncertainty over this region that is not apparent when focusing on one GCM-RCM combination. The CRCM5 driven by CanESM2 and MPI-ESM-LR suggest the frequency of freezing rain will decrease in the future with agreement among all algorithms, while the four algorithms applied to the CNRM-CM5- and GFDL-ESM2M-driven simulations show little agreement on the sign of change over this region.

Given the rarity of freezing rain, natural variability is also non-negligible. Though trends between simulations driven by the five members of the CanESM2 ensemble are generally similar, we find large regions of uncertainty on the sign of change over some regions. For example, even at +3°C of global warming, uncertainty on the sign of change persists over large regions of Québec. The irreducible nature of this uncertainty poses a challenge for future adaptation measures (e.g., Deser et al., 2012), and supports the use of large RCM ensembles like those examined in Jeong et al. (2019) for these events.

We have also identified regions where robust increases or decreases in freezing rain frequency are projected, regardless of algorithm selection or driving GCM. Our findings agree with those of previous studies on freezing rain under climate change, starting with Lambert and Hansen (2011), that the region of frequent freezing rain is likely to shift poleward in the future. At +2°C of global warming, we find strong agreement that freezing rain will become less frequent over the region of the eastern United States currently most commonly affected by freezing rain, from Texas northeastward to portions of coastal New England. The confidence in these projections and the magnitude of decrease strengthen at +3°C and +4°C of global warming, with strongest agreement over the southernmost portion of the projected decrease. This is likely related to the declining frequency of subfreezing surface temperatures necessary for freezing rain as the climate warms. Strong agreement in decreasing freezing rain frequency is also found over eastern Newfoundland, the region of North America where freezing rain is currently most frequent, related to warming surface temperatures.

At +2°C and especially +3°C of global warming, a clear signal of increasing freezing rain frequency emerges over the Canadian provinces of Alberta, Saskatchewan, and Manitoba, as well as in the Rocky Mountains of British Columbia. This region includes major cities such as Edmonton, Saskatoon, and Winnipeg. Given the potential impacts of freezing rain, further study of the details of this projected increase, for example, using additional models or techniques, is warranted. At +3°C, an additional region of projected increase emerges over Labrador and surrounding regions of Québec, though agreement is much weaker than over the aforementioned regions of western Canada.

Our results suggest that for studies interested in relative changes to freezing rain events, use of the Bourgouin (2000), Ramer (1993), and Baldwin and Contorno (1993) methods produce very similar projections. For applications requiring actionable information on potential freezing rain frequencies or amounts in the future climate, different algorithms may produce a broad range of values. As no perfect algorithm exists, presentation of results from multiple algorithms provides a better sense of the range of possible outcomes. However, certain algorithms and driving GCMs exhibit more skill at reproducing the recent past climatology of freezing rain than others (McCray, Thériault, et al. (2022)). Future studies may consider weighting the algorithms and driving GCMs based on their skill, rather than presenting basic arithmetic means as we have done here.

One important limitation of our research is that it relies on only one RCM, the CRCM5. The initial objective of this research included an examination of the results of other RCMs within the North American CORDEX ensemble, similar to the analysis performed by Kämäräinen et al. (2018) over Europe with EURO-CORDEX. However, lack of accessible sub-daily data on multiple vertical levels from other RCMs has complicated this endeavor. Given the substantial impacts of freezing rain events, modeling groups should consider archiving sub-daily temperature and humidity data on several vertical levels to allow for diagnosis of freezing rain from model output. The varying signals obtained from different driving GCMs in some regions highlight the need for a more complete analysis of a matrix of GCM-RCM combinations to gain a complete understanding of the level of certainty in projections of freezing rain events under climate change.

Finally, our study focuses solely on the changing annual climatology of freezing rain. As the climate warms, the annual frequency of freezing rain may decrease, but the occurrence of extreme events may increase at some locations. This is the case in some regions for snowfall, where annual snowfall is expected to decrease but extreme daily snowfall may remain constant or become more extreme as precipitation intensifies (e.g., O'Gorman, 2014). Because the highest impact freezing rain events are those that result in the greatest ice accretion, additional studies should also examine how these extremes may evolve in the future.

Data Availability Statement

Files containing annual freezing rain frequencies generated for each simulation and each precipitation-type algorithm can be found in McCray, Paquin, et al. (2022) (https://doi.org/10.20383/103.0575). Direct model output for all CRCM5 simulations examined here can be obtained by contacting scenarios@ouranos.ca. CMIP5 simulation output used for calculating global warming levels was downloaded from the Earth System Grid Federation (ESGF) portal hosted by the U.S. Department of Energy Lawrence Livermore National Laboratory (https://esgf-node.llnl.gov/search/cmip5/). Data can be accessed by selecting the appropriate model, ensemble member (r1i1p1 for all models plus r2i1p1–r5i1p1 for CanESM2), and variable *tas* for the *historical* and *rcp85* experiments at monthly frequency.

Acknowledgments
Funding for this work was provided via a Mitacs Accelerate grant, the first author's Fonds de recherche du Québec—Nature et technologies (FRQNT) postdoctoral research fellowship, Ouranos, and from J. Thériault's Canada Research Chair in Extreme Winter Weather Events and Natural Sciences and Engineering Research Council of Canada (NSERC) Discovery Grant. The CRCM5 simulations were produced by Ouranos on the Guillimin supercomputer at McGill University, managed by Calcul Québec and Compute Canada. Funding for Guillimin was provided by the Canada Foundation for Innovation (CFI), the ministère de l'Économie et de l'Innovation du Québec (MEI), and the FRQNT. The CRCM5 was developed at the Université du Québec à Montréal (UQAM) in collaboration with Environment and Climate Change Canada (ECCC).

References

Andrews, T., Gregory, J. M., Webb, M. J., & Taylor, K. E. (2012). Forcing, feedbacks and climate sensitivity in CMIP5 coupled atmosphere-ocean climate models. *Geophysical Research Letters*, *39*(9). https://doi.org/10.1029/2012GL051607

Arora, V. K., Scinocca, J. F., Boer, G. J., Christian, J. R., Denman, K. L., Flato, G. M., et al. (2011). Carbon emission limits required to satisfy future representative concentration pathways of greenhouse gases. *Geophysical Research Letters*, *38*(5). https://doi.org/10.1029/2010GL046270

Baldwin, M. E., & Contorno, S. (1993). *Development of a weather-type prediction system for NMC's mesoscale eta model*, Preprints, 13th Conf. on Weather Analysis and Forecasting, Vienna, VA, 86–87. Amer. Meteor. Soc.

Bocchieri, J. R. (1980). The objective use of upper air soundings to specify precipitation type. *Monthly Weather Review*, *108*(5), 596–603. https://doi.org/10.1175/1520-0493(1980)108<0596:tououa>2.0.co;2

Bourgouin, P. (2000). A method to determine precipitation types. *Weather and Forecasting*, *15*(5), 583–592. https://doi.org/10.1175/1520-0434(2000)015<0583:amtdpt>2.0.co;2

Bresson, E., Laprise, R., Paquin, D., Thériault, J. M., & de Elía, R. (2017). Evaluating the ability of CRCM5 to simulate mixed precipitation. *Atmosphere-Ocean*, *55*(2), 79–93. https://doi.org/10.1080/07055900.2017.1310084

Brooks, C. F. (1920). The nature of sleet and how it is formed. *Monthly Weather Review*, *48*(2), 69–72. https://doi.org/10.1175/1520-0493(1920)48<69b:tnosah>2.0.co;2

Cantin, A., & Bachand, D. (1993). *Synoptic pattern recognition and partial thickness techniques as a tool for precipitation types forecasting associated with a winter storm*. (Tech. Rep.). Centre Météorologique du Québec.

Changnon, S. A. (2003). Characteristics of ice storms in the United States. *Journal of Applied Meteorology*, *42*(5), 630–639. https://doi.org/10.1175/1520-0450(2003)042<0630:coisit>2.0.co;2

Cheng, C. S., Auld, H., Li, G., Klaassen, J., & Li, Q. (2007). Possible impacts of climate change on freezing rain in south-central Canada using downscaled future climate scenarios. *Natural Hazards and Earth System Sciences*, *7*(1), 71–87. https://doi.org/10.5194/nhess-7-71-2007

Cheng, C. S., Li, G., & Auld, H. (2011). Possible impacts of climate change on freezing rain using downscaled future climate scenarios: Updated for eastern Canada. *Atmosphere-Ocean*, *49*(1), 8–21. https://doi.org/10.1080/07055900.2011.555728

Cortinas, J. V., Bernstein, B. C., Robbins, C. C., & Strapp, J. W. (2004). An analysis of freezing rain, freezing drizzle, and ice pellets across the United States and Canada: 1976–90. *Weather and Forecasting*, *19*(2), 377–390. https://doi.org/10.1175/1520-0434(2004)019

Czys, R. R., Scott, R. W., Tang, K. C., Przybylinski, R. W., & Sabones, M. E. (1996). A physically based, nondimensional parameter for discriminating between locations of freezing rain and ice pellets. *Weather and Forecasting*, *11*(4), 591–598. https://doi.org/10.1175/1520-0434(1996)011<0591:apbnpf>2.0.co;2

DeGaetano, A. T. (2000). Climatic perspective and impacts of the 1998 northern New York and New England ice storm. *Bulletin of the American Meteorological Society*, *81*(2), 237–254. https://doi.org/10.1175/1520-0477(2000)081<0237:cpaiot>2.3.co;2

Deser, C., Knutti, R., Solomon, S., & Phillips, A. S. (2012). Communication of the role of natural variability in future North American climate. *Nature Climate Change*, *11*(2), 775–779. https://doi.org/10.1038/nclimate1562

Dunne, J. P., John, J. G., Adcroft, A. J., Griffies, S. M., Hallberg, R. W., Shevliakova, E., et al. (2012). GFDL's ESM2 global coupled climate-carbon Earth system models. Part I: Physical formulation and baseline simulation characteristics. *Journal of Climate*, *25*(19), 6646–6665. https://doi.org/10.1175/JCLI-D-11-00560.1

Giorgetta, M. A., Jungclaus, J., Reick, C. H., Legutke, S., Bader, J., Böttinger, M., et al. (2013). Climate and carbon cycle changes from 1850 to 2100 in MPI-ESM simulations for the coupled model intercomparison project phase 5. *Journal of Advances in Modeling Earth Systems*, *5*(3), 572–597. https://doi.org/10.1002/jame.20038

Hawkins, E., & Sutton, R. (2009). The potential to narrow uncertainty in regional climate predictions. *Bulletin of the American Meteorological Society*, *90*(8), 1095–1108. https://doi.org/10.1175/2009BAMS2607.1

Huffman, G. J., & Norman, G. A. (1988). The supercooled warm rain process and the specification of freezing precipitation. *Monthly Weather Review*, *116*(11), 2172–2182. https://doi.org/10.1175/1520-0493(1988)116<2172:tswrpa>2.0.co;2

IPCC. (2021). *Climate change 2021: The physical science basis. contribution of working group i to the sixth assessment report of the intergovernmental panel on climate change* [Masson-Delmotte, V., P. Zhai, A. Pirani, S. L. Connors, C. Péan, S. Berger, N. Caud, et al. (eds.)]. Cambridge University Press. https://www.ipcc.ch/report/ar6/wg1/downloads/report/IPCC_AR6_WGI_Citation.pdf

Jacob, D., Petersen, J., Eggert, B., Alias, A., Christensen, O. B., Bouwer, L. M., et al. (2014). Euro-cordex: New high-resolution climate change projections for European impact research. *Regional Environmental Change*, *14*(2), 563–578. https://doi.org/10.1007/s10113-013-0499-2

Jeong, D. I., Cannon, A. J., & Zhang, X. (2019). Projected changes to extreme freezing precipitation and design ice loads over North America based on a large ensemble of Canadian regional climate model simulations. *Natural Hazards and Earth System Sciences*, *19*(4), 857–872. https://doi.org/10.5194/nhess-19-857-2019

Jeong, D. I., Sushama, L., Vieira, M. J., & Koenig, K. A. (2018). Projected changes to extreme ice loads for overhead transmission lines across Canada. *Sustainable Cities and Society*, *39*, 639–649. https://doi.org/10.1016/J.SCS.2018.03.017

Kämäräinen, M., Hyvärinen, O., Vajda, A., Nikulin, G., van Meijgaard, E., Teichmann, C., et al. (2018). Estimates of present-day and future climatologies of freezing rain in Europe based on cordex regional climate models. *Journal of Geophysical Research: Atmospheres*, *123*(23), 13291–13304. https://doi.org/10.1029/2018JD029131

Klima, K., & Morgan, M. G. (2015). Ice storm frequencies in a warmer climate. *Climatic Change*, *133*(2), 209–222. https://doi.org/10.1007/S10584-015-1460-9/FIGURES/7

Kochtubajda, B., Mooney, C., & Stewart, R. (2017). Characteristics, atmospheric drivers and occurrence patterns of freezing precipitation and ice pellets over the Prairie Provinces and arctic territories of Canada: 1964–2005. *Atmospheric Research*, *191*, 115–127. https://doi.org/10.1016/J.ATMOSRES.2017.03.005

Lambert, S. J., & Hansen, B. K. (2011). Simulated changes in the freezing rain climatology of North America under global warming using a coupled climate model. *Atmosphere-Ocean*, *49*(3), 289–295. https://doi.org/10.1080/07055900.2011.607492

Lehner, F., Deser, C., Maher, N., Marotzke, J., Fischer, E. M., Brunner, L., et al. (2020). Partitioning climate projection uncertainty with multiple large ensembles and CMIP5/6. *Earth System Dynamics*, *11*(2), 491–508. https://doi.org/10.5194/ESD-11-491-2020

Martynov, A., Laprise, R., Sushama, L., Winger, K., Šeparović, L., & Dugas, B. (2013). Reanalysis-driven climate simulation over Cordex North America domain using the Canadian regional climate model, version 5: Model performance evaluation. *Climate Dynamics*, *41*(11–12), 2973–3005. https://doi.org/10.1007/s00382-013-1778-9

Matte, D., Thériault, J. M., & Laprise, R. (2018). Mixed precipitation occurrences over southern Québec, Canada, under warmer climate conditions using a regional climate model. *Climate Dynamics*, *53*(1–2), 1–17. https://doi.org/10.1007/s00382-018-4231-2

McCray, C. D., Atallah, E. H., & Gyakum, J. R. (2019). Long-duration freezing rain events over North America: Regional climatology and thermodynamic evolution. *Weather and Forecasting*, *34*(3), 665–681. https://doi.org/10.1175/WAF-D-18-0154.1

McCray, C. D., Gyakum, J. R., & Atallah, E. H. (2021). Synoptic–dynamic and airmass characteristics distinguishing long- and short-duration freezing rain events in the south-central United States. *Monthly Weather Review*, *149*(5), 1287–1304. https://doi.org/10.1175/MWR-D-20-0306.1

McCray, C. D., Paquin, D., Thériault, J. M., & Bresson, É. (2022). Annual frequencies of freezing rain diagnosed from the fifth-generation Canadian regional climate model (CRCM5) for the past and future climates [dataset]. Federated Research Data Repository. https://doi.org/10.20383/103.0575

McCray, C. D., Thériault, J. M., Paquin, D., & Bresson, É. (2022). Quantifying the impact of precipitation-type algorithm selection on the representation of freezing rain in an ensemble of regional climate model simulations. *Journal of Applied Meteorology and Climatology*. https://doi.org/10.1175/JAMC-D-21-0202.1

Meisinger, C. L. (1920). The precipitation of sleet and the formation of glaze in the eastern United States, January 20 to 25, 1920, with remarks on forecasting. *Monthly Weather Review*, *48*(2), 73–80. https://doi.org/10.1175/1520-0493(1920)48<73b:tposat>2.0.co;2

Mittermeier, M., Bresson, E., Paquin, D., & Ludwig, R. (2021). A deep learning approach for the identification of long-duration mixed precipitation in Montréal (Canada). *Atmosphere-Ocean*, 1–12. https://doi.org/10.1080/07055900.2021.1992341

Nikulin, G., Lennard, C., Dosio, A., Kjellström, E., Chen, Y., Hänsler, A., et al. (2018). The effects of 1.5 and 2 degrees of global warming on Africa in the cordex ensemble. *Environmental Research Letters*, *13*(6), 065003. https://doi.org/10.1088/1748-9326/AAB1B1

O'Gorman, P. A. (2014). Contrasting responses of mean and extreme snowfall to climate change. *Nature*, *512*(7515), 416–418. https://doi.org/10.1038/nature13625

Ramer, J. (1993). *An empirical technique for diagnosing precipitation type from model output*. Preprints, Fifth Int. Conf. on Aviation Weather Systems, Vienna, VA, Amer. Meteor. Soc. 227–230.

Rauber, R. M., Olthoff, L. S., Ramamurthy, M. K., & Kunkel, K. E. (2000). The relative importance of warm rain and melting processes in freezing precipitation events. *Journal of Applied Meteorology*, *39*(7), 1185–1195. https://doi.org/10.1175/1520-0450(2000)039<1185:triowr>2.0.co;2

Rauber, R. M., Olthoff, L. S., Ramamurthy, M. K., Miller, D., & Kunkel, K. E. (2001). A synoptic weather pattern and sounding-based climatology of freezing precipitation in the United States east of the Rocky Mountains. *Journal of Applied Meteorology*, *40*(10), 1724–1747. https://doi.org/10.1175/1520-0450(2001)040<1724:aswpas>2.0.co;2

Ressler, G. M., Milrad, S. M., Atallah, E. H., & Gyakum, J. R. (2012). Synoptic-scale analysis of freezing rain events in Montreal, Quebec, Canada. *Weather and Forecasting*, *27*(2), 362–378. https://doi.org/10.1175/WAF-D-11-00071.1

Scinocca, J. F., Kharin, V. V., Jiao, Y., Qian, M. W., Lazare, M., Solheim, L., et al. (2016). Coordinated global and regional climate modeling. *Journal of Climate*, *29*(1), 17–35. https://doi.org/10.1175/JCLI-D-15-0161.1

Scinocca, J. F., McFarlane, N. A., Lazare, M., Li, J., & Plummer, D. (2008). Technical note: The CCCMA third generation AGCM and its extension into the middle atmosphere. *Atmospheric Chemistry and Physics*, *8*(23), 7055–7074. https://doi.org/10.5194/ACP-8-7055-2008

Šeparović, L., Alexandru, A., Laprise, R., Martynov, A., Sushama, L., Winger, K., et al. (2013). Present climate and climate change over North America as simulated by the fifth-generation Canadian regional climate model. *Climate Dynamics*, *41*(11–12), 3167–3201. https://doi.org/10.1007/s00382-013-1737-5

St-Pierre, M., Thériault, J. M., & Paquin, D. (2019). Influence of the model horizontal resolution on atmospheric conditions leading to freezing rain in regional climate simulations. *Atmosphere-Ocean*, *57*(2), 101–119. https://doi.org/10.1080/07055900.2019.1583088

Voldoire, A., Sanchez-Gomez, E., Mélia, D. S., Decharme, B., Cassou, C., Sénési, S., et al. (2013). The CNRM-CM5.1 global climate model: Description and basic evaluation. *Climate Dynamics*, *40*(9–10), 2091–2121. https://doi.org/10.1007/s00382-011-1259-y